

NONLINEAR OPTICAL PHENOMENA

PACS numbers: 42.65.Jx; 42.65.Re; 33.80.Eh; 52.38.–r
DOI: 10.1070/QE2012v042n04ABEH014782

Nonlinear propagation of a high-power focused femtosecond laser pulse in air under atmospheric and reduced pressure

Yu.E. Geints, A.A. Zemlyanov, A.A. Ionin, S.I. Kudryashov,
L.V. Seleznev, D.V. Sinitsyn, E.S. Sunchugasheva

Abstract. **This paper examines the propagation of focused femtosecond gigawatt laser pulses in air under normal and reduced pressure in the case of Kerr self-focusing and photoionisation of the medium. The influence of gas density on the beam dimensions and power and the electron density in the plasma column in the nonlinear focus zone of the laser beam has been studied experimentally and by numerical simulation. It has been shown that, in rarefied air, the radiation-induced reduction in the rate of plasma formation diminishes the blocking effect of the plasma on the growth of the beam intensity in the case of tight focusing. This allows higher power densities of ultrashort laser pulses to be reached in the focal waist region in comparison with beam self-focusing under atmospheric pressure.**

Keywords: *femtosecond laser pulse, filament, plasma.*

1. Introduction

In optics, an increase in light intensity in a given volume of a medium is typically ensured by focusing a light beam with appropriate optical systems. The focusing of ultrashort laser pulses having a peak power of tens or hundreds of gigawatts offers the promise of reaching extreme intensities, approaching the level of intra-atomic power densities ($\sim 10^{15}$ W cm^{-2}) [1]. One serious impediment that is often encountered in this connection is optical nonlinearity of the medium where light propagates. The high peak power and intensity of femtosecond pulses may distort linear focusing before the target is reached [2]. The propagation of such light is accompanied by self-action: the beam experiences strong spatiotemporal self-modulation, which shows up as temporal pulse compression and subsequent transverse beam breakup into high-intensity regions – so-called beam filamentation (see, e.g., a review by Kandidov et al. [3] and references therein).

In air at atmospheric pressure, the main physical mechanism that prevents beam focusing and the associated increase in beam intensity is plasma formation [4]. Photoionisation of molecules leads to nonlinear energy losses in the beam channel and stops the increase in beam intensity caused by the initial focusing and Kerr self-focusing of the beam. The plasma forming at the leading edge of a laser pulse (with a free-electron density of 10^{22} to 10^{24} m^{-3}) defocuses the rest of the beam. This is accompanied by the formation of filaments: high-intensity regions of the laser pulse, localised in space (and time), whose size remains essentially constant over distances comparable to the initial beam diffraction length. In particular, for collimated Ti : sapphire laser pulses with a centre wavelength of about 800 nm, the average filament length is of the order of a hundred microns and the peak intensity in the filaments reaches 40–70 TW cm^{-2}.

Clearly, the adverse effect of the photoionisation of the medium on the propagation of a focusing laser beam can be reduced by raising the laser damage threshold of the medium, e.g. through the use of a gas with a high ionisation potential (in particular, argon [5] or neon) instead of air. This is however not always possible and not always technically or economically justified. Another way to solve this problem is to partially eliminate the cause of ionisation, i.e. to reduce the pressure in the beam waist zone. Lowering the air pressure reduces the number density of molecules and, hence, that of ionisation centres [6]. Accordingly, plasma-induced radiation blocking occurs later, and the beam intensity may exceed that under normal pressure.

The filamentation behaviour of high-power collimated ultrashort laser pulses in gases at different pressures was analysed by Couairon et al. [7] and Uryupina et al. [8], who presented experimental data and quantitative assessment of the effect of gas (air or argon) density on the spatiotemporal parameters and power of laser radiation in the filamentation zone. In particular, their results demonstrate that lowering the gas pressure has little effect on the peak radiation intensity in the filament. At the same time, recent work [9–13] has provided clear evidence that the self-focusing of a femtosecond laser pulse focused in air at atmospheric pressure has a number of special features. Beam focusing quality was shown to influence the cross-sectional size and length of filaments (but not their intensity) [13]. The behaviour of these parameters at reduced pressure remains unexplored.

In this work, using laboratory experiments and numerical simulation of the propagation of focusing femtosecond pulses of critical and subcritical power in air at different pressures, we establish a relationship between the focusing strength and parameters of a beam in its nonlinear focus region. We demonstrate that reducing the air pressure in the focusing zone may increase the maximum achievable laser pulse intensity by more than one order of magnitude.

Yu.E. Geints, A.A. Zemlyanov V.E. Zuev Institute of Atmospheric Optics, Siberian Branch, Russian Academy of Sciences, pl. Akad. Zueva 1, 634021 Tomsk, Russia; e-mail: ygeints@iao.ru;
A.A. Ionin, S.I. Kudryashov, L.V. Seleznev, D.V. Sinitsyn, E.S. Sunchugasheva P.N. Lebedev Physics Institute, Russian Academy of Sciences, Leninsky prosp. 53, 119991 Moscow, Russia

Received 1 December 2011
Kvantovaya Elektronika **42** (4) 319–326 (2012)
Translated by O.M. Tsarev

2. Theoretical model of ultrashort pulse propagation

Ultrashort laser pulse propagation was simulated using the nonlinear Schrödinger equation (NLSE). As shown in many studies (see e.g. reviews by Kandidov et al. [3] and Berge et al. [14]), this equation adequately describes all significant processes that influence an optical pulse propagating through a medium, at least at pulse durations no shorter than a few optical periods.

Below we consider the propagation of a predominantly focusing beam with a small diameter (of the order of millimetres) and an initial pulse duration of the order of a hundred femtoseconds, which is typical of most known laboratory self-focusing experiments. This leads to an optical path length no greater than a few metres, so the group velocity dispersion of the laser pulse will be neglected in subsequent calculations. For the same reason, the model we use makes no corrections for spatiotemporal focusing or self-steepening of the pulse.

Under these assumptions, the corresponding equation in a moving coordinate system fixed to the propagating pulse has the form

$$\left(\frac{\partial}{\partial z}-\frac{\mathrm{i}}{2n_0k_0}\nabla_\perp^2\right)U=\mathrm{i}k_0\left(n_2I-n_4I^2-\frac{N_\mathrm{e}}{2N_\mathrm{ecr}n_0}\right)U$$

$$-\left[\frac{\sigma_\mathrm{c}N_\mathrm{e}}{2}+\frac{\Psi_\mathrm{I}(I)}{2I}\Delta E_\mathrm{i}(N_0-N_\mathrm{e})\right]U. \qquad (1)$$

The pulse causes the free-electron concentration, N_e, in the beam channel (plasma density) to vary according to the equation

$$\frac{\partial N_\mathrm{e}}{\partial t}=\Psi_\mathrm{I}(I)(N_0-N_\mathrm{e})+\frac{\sigma_\mathrm{c}}{n_0\Delta E_\mathrm{i}}I-v_\mathrm{r}N_\mathrm{e}^2, \qquad (2)$$

which takes into account the multiphoton, tunnelling and cascade (impact) ionisation mechanisms and the decrease in free-electron concentration through electron–ion recombination. Here, $U(\boldsymbol{r}_\perp,z;t)$ is the slowly varying complex amplitude of the electric field of the light pulse; $\nabla_\perp^2$ is the transverse Laplacian; n_0 is the linear refractive index of the medium; $k_0=2\pi/\lambda_0$ is the wavenumber; $I=cn_0|U|^2/8\pi$ is intensity; n_2 and n_4 are the coefficients of the third-order (Kerr) and the next (saturating nonlinearity) nonlinear terms in the refractive index of the medium, $n=n_0+n_2I-n_4I^2$; $N_\mathrm{ecr}=1/(\sigma_\mathrm{c}\tau_\mathrm{c}c)$ is the critical electron density in the plasma; Ψ_I is the photoionisation rate (probability) in the medium; N_0 is the density of neutral atoms; σ_c, ΔE_i and τ_c are the cascade ionisation cross section of a molecule, its ionisation potential and the characteristic collision time of free electrons and heavy particles, respectively; v_r is the electron recombination rate; and c is the speed of light in vacuum.

Note that, taking into account earlier results [15], in Eqn (1) we neglect the inertial response of the Kerr effect, related to the rotational component of the cubic polarisability of gas molecules, and add a term responsible for the Kerr nonlinearity saturation at high light intensities.

In our numerical calculations, the input light was taken in the form of a focused beam having Gaussian transverse and temporal intensity profiles,

$$U(\boldsymbol{r}_\perp,z=0,t)=U_0\exp\left[-\frac{|\boldsymbol{r}_\perp|^2}{(2R_0)^2}-\frac{t^2}{(2t_\mathrm{p})^2}\right]\times$$

$$\times\exp\left[-\mathrm{i}k_0n_0|\boldsymbol{r}_\perp|^2\frac{\mathrm{NA}}{R_0}\right],$$

with a variable initial focusing parameter (numerical aperture), $\mathrm{NA}=R_0/f$, and a pulse peak power $P_0=(U_0R_0)^2cn_0/8=I_0\pi R_0^2$, where f, R_0, and t_p are the radius of curvature of the phase front, beam radius and 1/e pulse width, respectively. For definiteness, we took $R_0=1$ mm and $t_\mathrm{p}=100$ fs. The other parameters in (1) and (2) at $\lambda_0=800$ nm in air (80% N_2 + 20% O_2) under normal pressure (1 bar) were as follows: $n_2=3.2\times10^{-19}$ cm^2 W^{-1}, $n_4=2.5\times10^{-33}$ cm^4 W^{-2}, $\tau_\mathrm{c}=350$ fs, $\sigma_\mathrm{c}=5.52\times10^{-24}$ m^2, $v_\mathrm{r}=1.1\times10^{-12}$ m^3 s^{-1}, $\Delta E_\mathrm{i}(O_2)=12.1$ eV, $\Delta E_\mathrm{i}(N_2)=15.6$ eV, and $N_0=N_{0O_2}+N_{0N_2}$ with $N_{0O_2}=5\times10^{24}$ m^{-3} and $N_{0N_2}=2.1\times10^{25}$ m^{-3}. The critical power for self-focusing, $P_\mathrm{cr}=\lambda_0/(n_0k_0n_2)$, was thus 3.2 GW. The photoionisation rate of atoms, Ψ_I, was calculated in the Perelomov–Popov–Terent'ev (PPT) model [16]. Equation (2) was solved separately for oxygen and nitrogen, and the total free-electron concentration was found as the sum of the concentrations of the two gaseous species.

First, we present a preliminary qualitative analysis of the effect of gas pressure on the characteristics of the laser beam in the filamentation zone and the density of the forming plasma. The response of nonlinear light–medium interaction constants to changes in pressure, p, can be understood in terms of the density of neutral air molecules: $N_0(p)/N_0(p_0)=p/p_0$. Clearly, to a first approximation (neglecting the effect of pressure on interaction cross sections and the spectral width of molecular lines of gases [17]) we can take a simple model [7] in which all the nonlinear terms in the refractive index are proportional to pressure, $(n_2,n_4)\sim p/p_0$, and the electron mean free time depends inversely on pressure, $\tau_\mathrm{c}\sim p_0/p$. Therefore, with decreasing pressure the critical power for self-focusing increases, $P_\mathrm{cr}\sim p_0/p$, and accordingly the cascade ionisation cross section of the atoms decreases: $\sigma_\mathrm{c}=\omega_0^2\tau_\mathrm{c}/cN_\mathrm{ecr}(\omega_0^2\tau_\mathrm{c}^2+1)\sim p/p_0$ (provided that $\omega_0\tau_\mathrm{c}\gg1$).

The main parameters of filaments resulting from the self-focusing of an ultrashort laser pulse can be estimated using simple relations that directly follow from analysis of Eqns (1) and (2) [18]. Filamentation is due to physical mechanisms that prevent pulse collapse and stabilise the beam intensity: plasma formation and cubic nonlinearity saturation. The corresponding constraint of an instantaneous local balance between nonlinear light wave focusing and defocusing 'forces' is given by

$$n_2I_\mathrm{f}=n_4I_\mathrm{f}^2+\frac{N_\mathrm{ef}}{2N_\mathrm{ecr}n_0}, \qquad (3)$$

where I_f is a characteristic intensity of the optical field in the filament and $N_\mathrm{ef}=N_\mathrm{e}(I_\mathrm{f})$ is a characteristic electron density in the plasma column. Physically, this relation can be interpreted as the condition that the phase shift of an optical wave at a given point in space and time through the action of the nonlinear light self-modulation mechanisms chosen should be zero.

The parameter N_ef in the vicinity of a filament can be roughly estimated using Eqn (2), where for simplicity the pho-

toionisation of gas molecules is treated in terms of the multiphoton absorption (MPA) mechanism, that is, under the assumption that $\Psi_I(I) = \sigma^{(K)} I^K$, where $\sigma^{(K)}$ is the MPA cross section and K is the number of photons needed to remove one electron from a neutral species ($K = 8$ for O_2 and $K = 11$ for N_2).

Neglecting free-electron recombination, we find that, when propagating through a gaseous medium, a laser pulse of intensity I_f and duration t_p, with a rectangular temporal profile, produces $N_{ef} = N_0 v_c^{-1} \sigma^{(K)} I_f^{K-1} [\exp(v_c I_f t_p) - 1]$ negatively charged particles per unit volume of the medium, where $v_c = \sigma_c/(n_0 \Delta E_i)$ is the cascade ionisation rate coefficient, and $N_e \ll N_0$. Since in the case of gases and femtosecond pulses the exponent in the above expression is typically much less than unity, we obtain the obvious relation

$$N_{ef} \approx N_0(p) t_p \sigma^{(K)} I_f^K, \tag{4}$$

from which the pressure dependence of the parameters of interest is clear. Substituting (4) into (3), neglecting the term containing n_4 (for $I_f < n_2/n_4$) and solving for I_f, we obtain an estimate of the mean optical field intensity in the filament:

$$I_f = \left[\frac{2 n_2(p) n_0 N_{ecr}}{N_0(p) t_p \sigma^{(K)}} \right]^{1/(K-1)}. \tag{5}$$

From the condition that the average power in the filament, $P_f = \pi I_f R_f^2$, be roughly equal to the critical power for self-focusing, P_{cr} [19], it follows that the characteristic filament radius is

$$R_f = k_0^{-1} \sqrt{\frac{2}{n_0 n_2(p) I_f}}. \tag{6}$$

Thus, if a laser pulse propagating through a medium under normal pressure undergoes Kerr self-focusing followed by intensity stabilisation in the filament at the level of I_f due to plasma formation near the beam waist, filamentation in a rarefied gas occurs at the same characteristic intensity but at a lower electron density, as follows from (4)–(6). The filament size then should increase because of the increase in the critical power for self-focusing. It should be emphasised that the above reasoning applies to collimated light.

It is quite clear that, because $P_{cr} \sim p_0/p$, a light pulse that has a supercritical power $P_0 > P_{cr}$ under normal conditions and, hence, undergoes self-focusing may become subcritical ($P_0 < P_{cr}$) with decreasing pressure and undergo no self-focusing, because the pulse power may be insufficient for overcoming the natural diffraction divergence of the beam due to the Kerr effect. As shown below, a radically different situation may occur if the beam is focused from the beginning. In this case, even for a subcritical pulse propagating in rarefied air, an increase in beam intensity, plasma formation and filamentation are possible. Moreover, it is seen from (2) that lowering the pressure reduces the total rate of gas ionisation (through both the multiphoton and cascade mechanisms) and, hence, the instantaneous concentration of free electrons generated by the laser pulse. The blocking effect of the plasma diminishes and as a result the intensity at the beam waist may exceed that under normal pressure.

3. Discussion of the numerical-simulation results

To analyse in greater detail the effect of air pressure on the characteristics of the filament and plasma column resulting from the self-focusing of ultrashort laser pulses, we performed a series of numerical calculations using Eqns (1) and (2). The curves in Fig. 1 illustrate the effect of beam focusing quality (quantified by the numerical aperture of the beam, NA) on the maximum achievable laser pulse intensity, I_{max}, and the free-electron density in the plasma, $N_{e\,max}$, in the nonlinear focus zone. Subcritical pulses and pulses with the critical peak power for self-focusing (under normal pressure) are considered separately. At the beam parameters chosen, these correspond to total pulse energies $E_0 = 56$ (Figs 1a, 1c) and 560 μJ (Figs 1b, 1d). In all the figures in this paper, points represent numerical-simulation results and lines, drawn as a guide to the eye, represent spline fits.

It follows from Fig. 1 that, at a subcritical pulse power, increasing the beam focusing strength is accompanied by an increase in maximum intensity in the focal region. Below NA $\sim 2 \times 10^{-3}$ (in what follows, this value will be considered a hypothetical boundary between weak and tight beam focusing modes), this increase corresponds to linear focusing propagation, where $I_{max} \propto NA^{-2}$ [curves (*3*) in Figs 1a and 1b, corresponding to propagation in vacuum]. At higher NA values, the intensity rises more gradually because of the plasma formation in the focal region. One exception is beam self-focusing at $P_0 = P_{cr}$ under normal pressure [Fig. 1b, curve (*1*)], which leads to filament formation with an intensity varying only slightly with focusing parameter: $I_{max} \approx 50$ TW cm^{-2}.

A decrease in air pressure has, on the whole, the same effect on I_{max} at subcritical pulse powers and at the critical value: the maximum achievable intensity at the nonlinear beam focus increases. This occurs at NA values corresponding to sufficiently tight beam focusing (NA $> 10^{-3}$) and is due to the reduction in the rate of plasma formation with decreasing gas pressure. In addition, the blocking effect of the plasma on the growth of the focusing beam intensity diminishes, which allows the beam to contract and its intensity to easily reach higher values at the beam waist.

This is the main distinction of the self-action of a tightly focused beam from the self-focusing of a collimated (or weakly focused) beam, which is usually due only to the Kerr effect. As shown above [see relation (5)], in the latter instance the limiting peak intensity level in the extended nonlinear focus (filament) zone is ensured not by beam filament but by the balance between the Kerr and plasma nonlinearities and is independent of gas pressure [20]. The formation of such a light filament with a quasi-constant peak intensity is well illustrated by curve (*1*) in Fig. 1b at low NA values.

It is important to note that lowering the gas pressure has a stronger effect on the growth of the maximum achievable laser pulse intensity at the critical power, raising I_{max} by more than one order of magnitude. At $P_0 = 0.1 P_{cr}$ (Fig. 1a), the growth is considerably smaller: by about a factor of 2.

At the same time, the peak free-electron density in the filament zone varies with gas pressure in the opposite way: $N_{e\,max}$ decreases with decreasing pressure. In the two situations under consideration (Figs 1c, 1d), the ratio of the maximum achievable plasma densities at different pressures meets the relation $N_{e\,max}(p_1)/N_{e\,max}(p_2) \backsim p_1/p_2$ [cf. (4)] at any NA value except for the filamentation-free region at NA $< 10^{-3}$ and

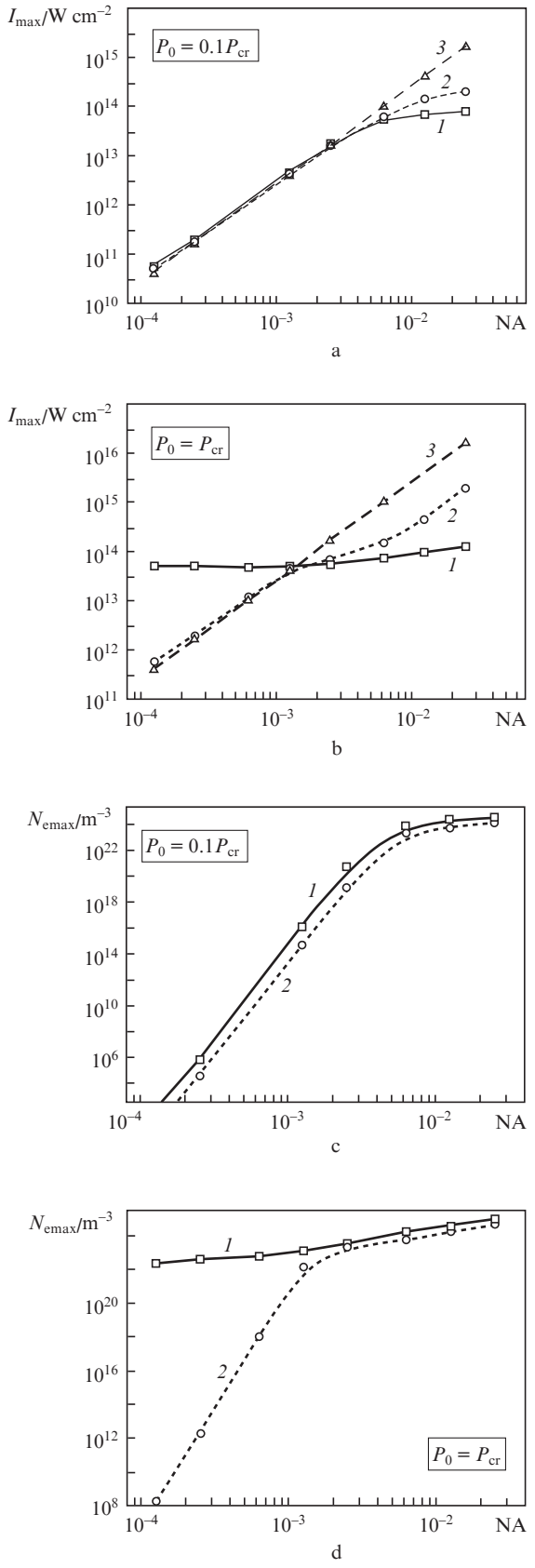

Figure 1. (a, b) Maximum achievable intensity, I_{max}, and (c, d) free-electron density in the plasma, N_{emax}, as functions of focusing parameter, NA, for femtosecond laser pulses at air pressures $p = (1)$ 1, (2) 0.1 and (3) 0 bar and subcritical initial pulse powers (a, c) $P_0 = 0.1P_{cr}$ and (b, d) $P_0 = P_{cr}$ (under normal pressure).

E_0 = 560 μJ. Accordingly, the pulse energy loss at the beam waist also decreases with decreasing pressure (Fig. 2).

The extremum in E(NA) at $P_0 = P_{cr}$ and normal pressure (Fig. 2b) is due to the transition from one beam filamentation regime to another. The right part of the curve (relative to the maximum, i.e. for NA > 2×10^{-3}) corresponds to beam contraction towards the waist due primarily to only linear diffraction, which is caused by the initial phase front curvature. Kerr self-focusing shows up here only in the beam waist region, elongating it (relative to its linear size) [11, 12]. The associated rise in pulse energy losses is due to the increase in free-electron gas density through developing avalanche ionisation of gas molecules.

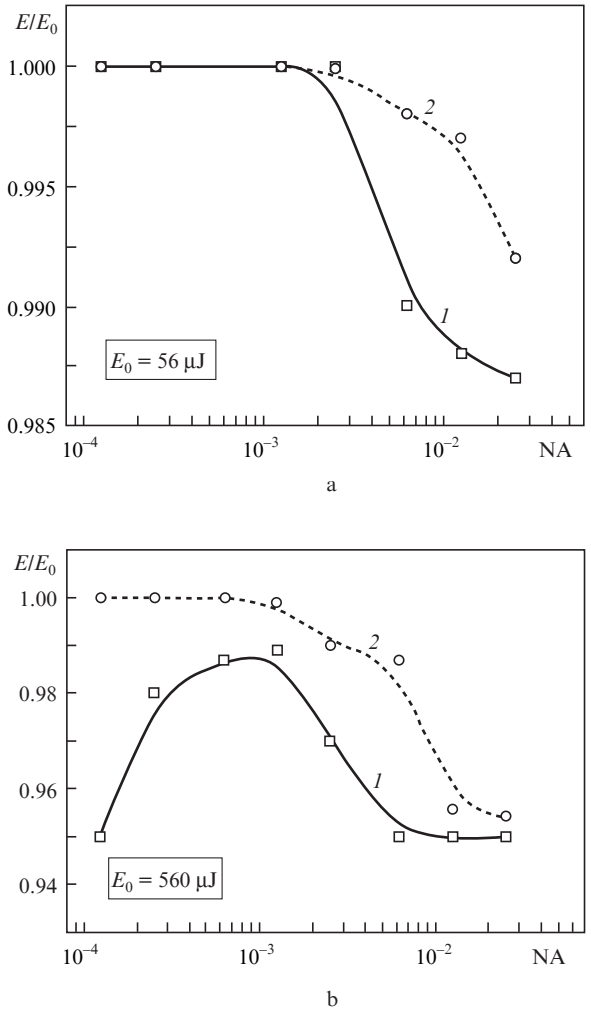

Figure 2. Normalised laser pulse energy, E/E_0, behind the focal waist as a function of focusing parameter, NA, at air pressures $p = (1)$ 1 and (2) 0.1 bar and initial pulse energies E_0 = (a) 56 and (b) 560 μJ.

In the case of weak beam focusing (NA < 2×10^{-3}), the influence of the cubic nonlinearity of the medium begins to show up well before the linear beam waist. This leads to axial filament formation with plasma densities considerably lower than above, even though at a high peak intensity. At the same time, the plasma column is then long enough to ensure significant pulse energy losses in its region.

The effect of gas pressure on the transverse size of the forming filament and the length of the plasma column is illus-

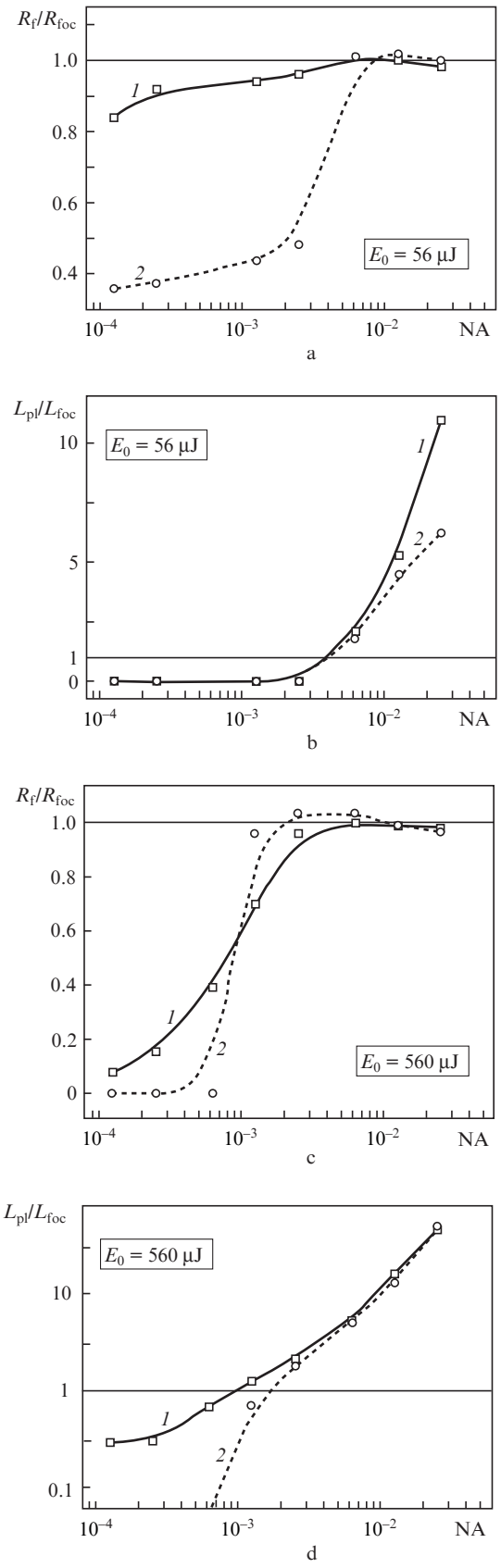

Figure 3. (a, c) Relative beam radius at the nonlinear focus and (b, d) effective plasma column length as functions of focusing parameter, NA, at air pressures p = (*1*) 1 and (*2*) 0.1 bar and initial pulse energies E_0 = (a, b) 56 and (c, d) 560 μJ.

trated by Fig. 3, which shows the relative (normalised) filament radius R_f/R_{foc} and effective plasma region length L_{pl}/L_{foc} as functions of the beam focusing parameter. The variables are normalised to the radius, $R_{foc} = R_0\gamma_D[\gamma_D^2 + NA^2]^{-1/2}$, and effective length, $L_{foc} \backsim 2k_0R_{foc}^2$, of the Gaussian beam waist in vacuum, where $\gamma_D = (k_0 R_0)^{-1}$ is the natural (diffraction-limited) angular divergence. In numerical simulations, R_f and L_{pl} were calculated from appropriate beam intensity and free-electron density data. As the plasma column length we took the evolution variable interval where the constraint $N_{emax} \geqslant 10^{21}$ m^{-3} was satisfied, and as the filament radius we took the minimum radius (at the 1/e level) over the entire beam waist length.

It is seen in Fig. 3 that, in the case of a tightly focused beam, lowering the gas pressure by an order of magnitude reduces the plasma column length to the extent that it disappears at low NA values. An essential point is that, in addition, the filament radius increases (only slightly), as predicted by relation (6).

On the whole, the beam radius in the filamentation region is a nonmonotonic function of beam focusing parameter at any air pressure. For a weakly focused beam, the transverse filament size, R_f, is smaller than the linear beam waist radius and tends to increase with increasing focusing parameter. In the case of moderate focusing [NA $\approx (2-5) \times 10^{-3}$], the cross section of the filament covers almost the entire linear waist area. This suggests that the transverse Gaussian energy density profile of the laser pulse in the beam waist region remains unchanged and that, therefore, the pulse self-steepening due to Kerr self-focusing during filament development has no significant effect on the process [12]. As the beam focusing parameter increases further (NA $> 5 \times 10^{-3}$), the variation in the filament radius follows that in the beam waist size, which corresponds to the saturation of the curves in Figs 3a and 3c near unity.

However, even though the approximate equality $R_f \approx R_{foc}$ is valid in this range of focusing parameters, it is quite reasonable to expect that filamentation occurs in this case as well. Indeed, even with tight beam focusing, the length of the nonlinear focus zone, where the beam has the highest intensity, exceeds the linear dimensions of the focal waist by more than one order of magnitude (Figs 3b, 3d). This corresponds to the known fact that filaments grow from the geometric focus of the beam in the direction opposite to the beam direction [21] because the beginning of a filament is the nonlinear focus of the pulse, which forms before its geometric focus. This circumstance, as well as the high degree of ionisation of the medium, suggests that, in the case of a tightly focused beam as well, a filament forms in the vicinity of the geometric focus of the beam.

4. Experimental procedure and results

Parameters of the focal zone of ultrashort laser pulses under tight focusing conditions in air at various pressures were determined experimentally using a femtosecond Ti:sapphire laser system (Avesta), which generates 100-fs (FWHM) pulses at 744 nm with a 10-Hz repetition frequency. In our experiments, we used laser pulses with a peak power P_0 no greater than a few times the critical power for self-focusing, P_{cr}, and an energy E_0 no higher than 1.9 mJ. The 1/e beam radius at the laser system output was 4 mm. A schematic of the experimental configuration is shown in Fig. 4.

At the output of the laser system (*1*), we placed a diffraction attenuator (*2*) (Institute of Automation and Electrometry, Siberian Branch, Russian Academy of Sciences), which enabled laser pulse energy measurements in the range 5 μJ to 1.9 mJ. After the diffraction attenuator, a beam splitter (*3*) directed a small part (~5%) of the beam to an Ophir calorimeter (*4*), which measured the pulse energy. After the beam splitter, the pulse was focused by a lens (*5*). In our experiments, we employed lenses with focal lengths $f = 80$, 130, 180 and 380 mm and an $f = 1100$ mm spherical mirror, which yielded numerical apertures NA ≈ 0.05, 0.03, 0.02, 0.01 and 0.004, respectively.

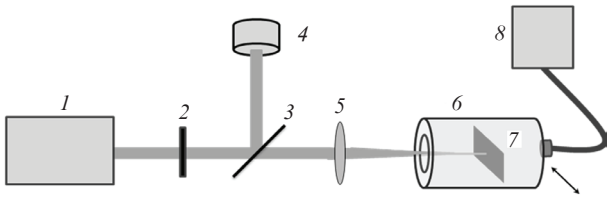

Figure 4. Optical layout of the experimental setup: (*1*) laser system, (*2*) diffraction attenuator, (*3*) beam splitter, (*4*) calorimeter, (*5*) lens, (*6*) travelling vacuum chamber, (*7*) thermosensitive paper, (*8*) vacuum pump.

On a motor-controlled positioning system in the focal region was placed a vacuum chamber (*6*) with thermosensitive paper (*7*), which were translated at an angle to the optical axis. As a result of such translation, a series of burn spots were produced on the paper (Fig. 5). The laser beam was slightly elliptical, which allowed the position of the focus to be determined rather accurately from the rotation of the axes of the ellipse. The burn spot area S was measured on a Levenhook Bio View 630 optical microscope at a preset paper blackening contrast level, which corresponded to a (constant) threshold laser energy density, w_{th}. The $S(P_0, \mathrm{NA}, p)$ data set was then used to calculate the effective peak beam intensity at the focal waist, $\bar{I}_f$.

The energy density distribution across the focal spot of the laser beam was assumed to be Gaussian:

$$w_{th} = w_{peak}(P_0, z = f)\exp\left[-\frac{S}{S_0(P_0, z = f)}\right], \tag{7}$$

where w_{peak} and S_0 are unknown parameters of the distribution. This assumption is valid when the pulse power is only slightly above the critical power for self-focusing and the initial beam focusing is sufficiently tight [11]. The peak pulse energy density, w_{peak}, can be expressed through the initial pulse power under the assumption that the temporal pulse profile remains unchanged and that there are no energy losses until the focus is reached:

$$w_{peak} = \frac{1}{S_0}\int_0^\infty P(t.z = f)\mathrm{d}t \approx \frac{bP_0}{S_0} = b\bar{I}_f, \tag{8}$$

where b is the integral of the temporal pulse profile (non-Gaussian in general). Therefore, to evaluate the effective intensity $\bar{I}_f$, one should know the characteristic beam area S_0 at the focal point.

In the case of linear beam focusing, S_0 at $z = f$ can be expressed through the numerical aperture parameter $S_{0L} = \pi(k_0\mathrm{NA})^{-2}$, and we have

$$\bar{I}_f \equiv I_{fL} = \frac{P_0(k_0\mathrm{NA})^2}{\pi}.$$

As a result of the multiphoton gas ionisation, maintained by Kerr self-focusing, and plasma generation, S_0 depends on laser pulse power:

$$S_0(P_0) = S_{0L} + P_0\partial_P S_0 = S_{0L} + \partial_{\ln P} S_0, \tag{9}$$

where $\partial_x \equiv \partial/\partial x$. It is clear from the above analysis that $S_0 \geqslant S_{0L}$, i.e. the effective focal spot area under plasma formation conditions can only increase relative to the beam waist area in vacuum. Consequently, under the above assumptions the pulse intensity at the focus must be lower than I_{fL}.

Using (7)–(9), we find a relation between changes in the burn spot area on the paper and S_0:

$$\partial_{\ln P} S = S_{0L} + \partial_{\ln P} S_0 \ln\left(\frac{bP_0}{w_{th} S_{0L}}\right).$$

Thus, knowing S_{0L} and evaluating the slope of the measured burn spot area, S, as a function of the logarithm of the pulse power, $\ln P_0$, we find the nonlinear increment of the beam area, $\partial_{\ln P} S_0$, and finally the effective intensity $\bar{I}_f$. The estimates below were made for a Gaussian temporal beam profile, which yielded $b = \sqrt{\pi}\, t_p$. The burn threshold of the photo

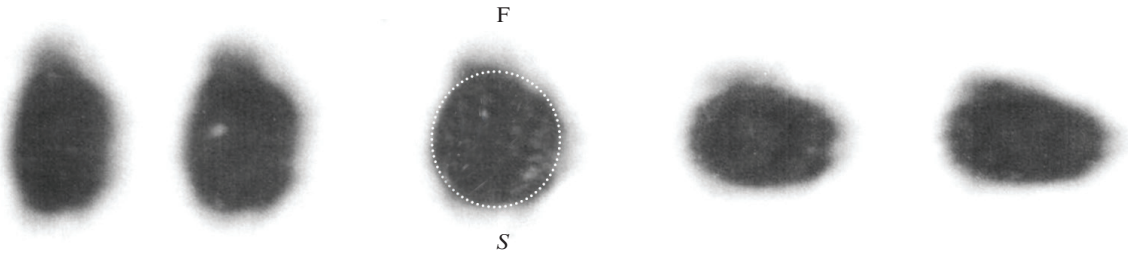

Figure 5. Series of burn spots on thermosensitive paper (F marks the burn spot corresponding to the focus of the lens; S is the burn spot area).

paper, $I_{th} = w_{th}/b$, determined at the minimum laser pulse energy (5 μJ), is ~2 GW cm^{-2}.

Figure 6a shows the effective focal intensity as a function of laser output power at atmospheric pressure for various numerical apertures. All the curves are seen to be quasi-linear up to $P_0 \approx 2$ GW. At higher pulse powers, the intensity increases in most cases more gradually, which is attributable to the formation of a dense plasma as a result of high-intensity laser exposure and pulse self-diffraction from the forming plasma column. With increasing numerical aperture, the peak intensity increases, reaching $\bar{I}_f \sim 10^{13}$ W cm^{-2} at P_0 near $3P_{cr}$ and NA = 0.004. In the case of tighter focusing (NA = 0.05), it may reach 1.3×10^{14} W cm^{-2}.

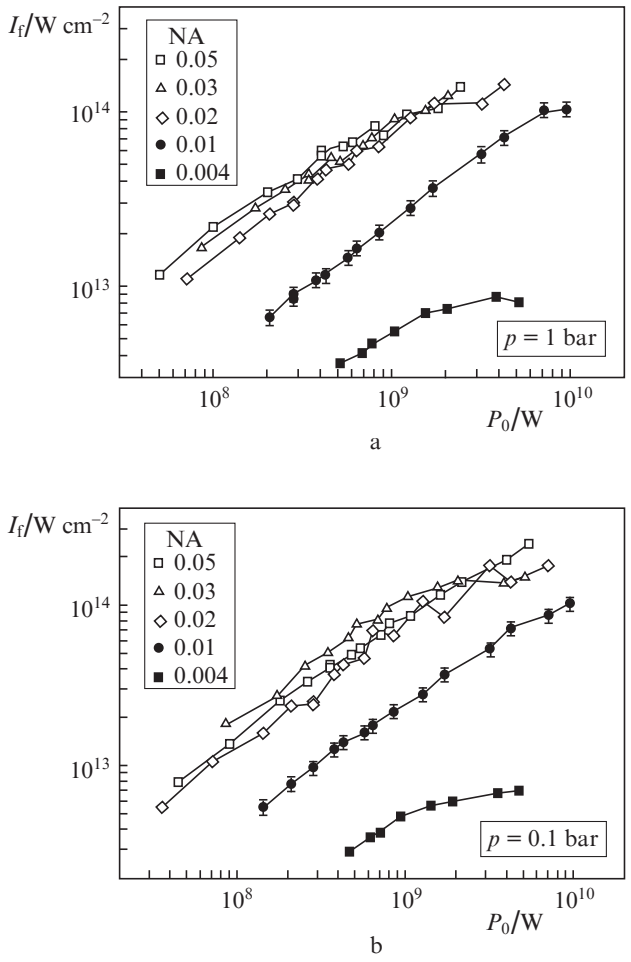

Figure 6. Effective peak laser pulse intensity at the focal waist as a function of initial power at various numerical apertures and air pressures p = (a) 1 and (b) 0.1 bar.

Figure 6b shows the effective peak intensity as a function of laser output power at a pressure of 10% of atmospheric pressure for various numerical apertures. Like at $p = 1$ bar, the intensity increases with increasing focusing parameter, NA, and varies little starting at NA = 0.02. The curves in Fig. 6b differ from those obtained at atmospheric pressure in that the intensity increases considerably when the beam is tightly focused and the pulse power exceeds the critical power for self-focusing, P_{cr} (under normal conditions). The maximum achievable intensity, $\bar{I}_f$, at a reduced pressure $p = 0.1$ bar and NA = 0.05 is ~2.4×10^{14} W cm^{-2}, in good agreement with the numerical simulation results for I_{max} (Figs 1a, 1b).

5. Conclusions

General aspects of the Kerr self-focusing and filamentation of femtosecond laser pulses propagating in air under normal and reduced pressure have been studied theoretically and experimentally as a function of initial spatial beam focusing. Analysis of numerical simulation results and experimental data indicates that, at a given laser pulse power, lowering the gas pressure changes beam self-focusing conditions and may prevent filamentation. At the same time, increasing the beam focusing strength (numerical aperture) may lead to the formation of a filament whose cross-sectional size approaches the linear beam waist radius and whose length exceeds it by an order of magnitude. In rarefied air, the free-electron concentration increases more gradually, which reduces the blocking effect of the plasma on the growth of the beam intensity in the case of tight focusing and allows higher intensities to be reached in the beam waist region. A factor of 10 decrease in air pressure in the focal zone may increase the maximum achievable laser pulse intensity at the critical power by more than one order of magnitude (to ~240 TW cm^{-2}) relative to the intensity in the case of collimated beam self-focusing under normal conditions.

Acknowledgements. This work was supported in part by the Russian Foundation for Basic Research (Grant Nos 09-05-00738-a, 11-02-12061, 10-02-01477 and 11-02-01100) and the International Science and Technology Center (Grant No. 4073).

References

1. Bukin V.V., Vorob'ev N.S., Garnov S.V., Konov V.I., Lozovoi V.I., Malyutin A.A., Shchelev M.Ya., Yatskovskii I.S. *Kvantovaya Elektron.*, **36**, 638 (2006) [*Quantum Electron.*, **36**, 638 (2006)].
2. Geints Yu.E., Zemlyanov A.A. *Opt. Atmos. Okeana*, **21**, 793 (2008).
3. Kandidov V.P., Shlenov S.A., Kosareva O.G. *Kvantovaya Elektron.*, **39**, 205 (2009) [*Quantum Electron.*, **39**, 205 (2009)].
4. Polynkin P., Kolesik M., Wright E.M., Moloney J.V. arXiv:1010.2303v1 [physics.optics] (2011).
5. Liu W., Bernhardt J., Theberge F., Chin S.L., Châteauneuf M., Dubois J. *J. Appl. Phys.*, **102**, 033111 (2007).
6. Kandidov V.P., Kosareva O.G., Shlenov S.A. *Kvantovaya Elektron.*, **21**, 971 (1994) [*Quantum Electron.*, **24**, 905 (1994)].
7. Couairon A., Franco M., Mechain G., Olivier N., Prade B., Mysyrowicz A. *Opt. Commun.*, **256**, 265 (2006).
8. Uryupina D., Kurilova M., Mazhorova A., Panov N., Volkov R., Gorgutsa S., Kosareva O., Savel'ev A., Chin S.L. *J. Opt. Soc. Am. B*, **27**, 667 (2010).
9. Theberge F., Liu W., Simard P., Becker A., Chin S.L. *Phys. Rev. E*, **74**, 036406 (2006).
10. Ionin A.A., Kudryashov S.I., Makarov S.V., Seleznev L.V., Sinitsyn D.V. *Pis'ma Zh. Eksp. Teor. Fiz.*, **90**, 467 (2009).
11. Geints Yu.E., Zemlyanov A.A., Ionin A.A., Kudryashov S.I., Seleznev L.V., Sinitsyn D.V., Sunchugasheva E.S. *Zh. Eksp. Teor. Fiz.*, **138**, 822 (2010).
12. Geints Yu.E., Zemlyanov A.A. *Opt. Atmos. Okeana*, **23**, 274 (2010).
13. Kosareva O.G., Liu W., Panov N.A., Bernhardt J., Ji Z., Sharifi M., Li R., Xu Z., Liu J., Wang Z., Ju J., Lu X., Jiang Y., Leng Y., Liang X. *Laser Phys.*, **19**, 1776 (2009).

14. Berge L., Skupin S., Nuter R., Kasparian J., Wolf J.-P. *Rep. Prog. Phys*., **70**, 1633 (2007).
15. Geints Yu.E., Zemlyanov A.A., Kabanov A.M., Matvienko G.G., Stepanov A.N. *Opt. Atmos. Okeana*, **22**, 119 (2009).
16. Perelomov A.M., Popov V.S., Terent'ev M.V. *Zh. Eksp. Teor. Fiz*., **50**, 1393 (1966).
17. Ignat'ev A.B., Morozov V.V. *Opt. Atmos. Okeana*, **14**, 413 (2001).
18. Geints Yu.E., Zemlyanov A.A. *Kvantovaya Elektron*., **40**, 121 (2010) [*Quantum Electron*., **40**, 121 (2010)].
19. Braun A., Korn G., Liu X., Du D., Squier J., Mourou G. *Opt. Lett*., **20**, 75 (1995).
20. Bernhardt J., Liu W., Chin S.L., Sauerbrey R. *Appl. Phys. B*, **91**, 48 (2008).
21. Bagaev S.N., Geints Yu.E., Zemlyanov A.A., Kabanov A.M., Matvienko G.G., Pestryakov E..V., Stepanov A.N., Trunov V.I. *Opt. Atmos. Okeana*, **20**, 413 (2007).